INFLUENCE OF ANODIZATION TEMPERATURE ON THE STRUCTURAL FEATURES OF FIRST-STEP ANODIZED NANOPOROUS ALUMINA AND OF COMMERCIAL ALUMINIUM SUBSTRATE

S. M. JUNAID ZAIDI[a], M. Z. BUTT[b*]
[a] *Department of Physics, GC University, Lahore-54000, Pakistan*
[b] *Centre for Advanced Studies in Physics, GC University, Lahore 54000, Pakistan*

First-step anodization of commercial aluminium in 0.3 M oxalic acid at 50 V for 15 min was investigated at –10, –5, 0, 20, and 30 $^{\circ}$C. Current – time transient plots of the specimens were recorded via computer interfaced multimeter to analyze oxidation and reduction behavior during the experiment. It is found that current density, charge transferred, and thickness of nanoporous alumina film increase exponentially with anodization temperature. The activation energy of the rate process of anodization determined from the Arrhenius plots of current density, charge transferred, and film thickness is found to be 0.182 eV with a standard deviation of 0.007 eV. Influence of anodization temperature on the structural features of nanoporous alumina and of commercial aluminium substrate was examined by SEM and XRD. Pore diameter, interpore distance, and porosity increase whereas pore circularity and pore density decrease linearly with the increase in anodization temperature. The intensity of diffraction peak pertaining to preferentially oriented crystallographic plane (311) of commercial aluminium substrate decreases whereas its FWHM increases at all anodization temperatures. The observations are in qualitative agreement with those reported in the literature for high-purity aluminium.

1. Introduction

Recently porous anodic aluminium oxide (AAO) films have gained much attention for the fabrication of structural nano-materials. These films can be fabricated on pure aluminum substrate by the process of anodization. In this process, aluminum metal is placed at anode in an electrolyte, which can be acidic, e.g. oxalic acid, sulphuric acid, and phosphoric acid [1-3], etc. or basic, e.g. sodium hydroxide [4] etc. Porous AAO is renowned for its good mechanical, thermal, and chemical stability, excellent dielectric properties, low hardness, and controllable pore diameter and interpore distance. It has enormous applications as biosensors [5], hemodialysis devices [6], nano-pores template [7], conductive substrate [8], supercapicators [9].

Several anodization methods have been adopted to grow metal oxide films on pure metal surface, such as one-step or mild anodization at low voltage [10], two-step anodization [11], hard anodization at low temperature and high voltage [3], pulsed anodization [12], and plasma anodization [13], etc. The growth of AAO film depends upon various anodization parameters during experiment, like anodization voltage, time, temperature [11, 14, 15], as well as concentration and nature of electrolyte [16].

The temperature of the electrolyte at which anodization of metals is carried out influences not only thickness of the oxide layer but also its structural features. For instance, Sulka and Stepniowski [17] studied the effect of relatively high temperatures (20, 25, 30 $^{\circ}$C) on the anodization of 5N+ pure aluminium in 0.3M oxalic acid ($C_2H_2O_4$) at different anodizing potentials in the range 30 to 65 V with an interval of 5 V. They found that for each anodizing voltage,

---

[*]Corresponding author: mzakriabutt@gmail.com

various parameters namely current density, oxide layer thickness, pore diameter, interpore distance and porosity increase with temperature whereas pore density decreases. Moreover, Stepniowski and Bojar [11] developed nanoporous alumina by anodization of 5N+ pure aluminium in 0.3M oxalic acid at still higher four temperatures (35, 40, 45, 50°C) under constant cell voltage ranging from 20 to 60 V. The time of anodization was 30, 60, or 120 min for a given specimen. They found that pore diameter increases with anodizing voltage, temperature and duration of the anodizing step. However, interpore distance is influenced only by the anodizing potential, and remains un-influenced by temperature or time of anodization.

The main purpose of the present research work was to fabricate porous AAO films on commercial purity rather than on expensive 5N+ pure aluminum substrate in an electrolyte of 0.3 M oxalic acid at 50 V for 15 min at five different temperatures in the range −10 to +30 $^{\circ}$C. Another objective was to investigate the effect of anodization temperature on the current – time response, current density of anodization, AAO film thickness, activation energy of rate process of anodization, and various structural parameters, namely pore diameter, pore circularity, interpore distance, pore density, and porosity, etc. of nanoporous alumina films. Furthermore, structural changes occurred in the aluminium substrate on anodization, not reported in the literature before, will also be investigated in detail.

2. Experimental work

Six square-shape specimens (1.5 cm × 1.5 cm) of 1 mm thickness were cut from a commercially pure aluminium sheet. The specimens were pre-heated at 450 $^{\circ}$C for 3 hours to remove internal stresses. After mechanical polishing, the specimens were electro-polished in the designed setup. Five specimens were then anodized in an electrolyte of 0.3 M oxalic acid in an anodization chamber at 50 V for 15 min at five different temperatures in the range − 10 to + 30°C, and sixth specimen was kept un-anodized for reference purpose. The electrolyte was stirred vigorously during anodization for uniform temperature distribution. The value of current was recorded throughout the anodization period with the help of software of computer interfaced multimeter.

3. Results and discussion

3.1. Current - time response

Fig. 1 represents current - time plots of Al specimens anodized at - 10, - 5, 0, 20, and 30 $^{\circ}$C. One can see that after a sudden increase in current due to movement of electrolyte ions towards anode on the application of voltage, the current is then sharply decreased due to oxide layer formation on the specimen surface, and is later on stabilized due to equilibrium between oxidation and reduction process during anodization. It is worthy of mention that the current – time plot of specimen anodized at 20 $^{\circ}$C represent rather large distortion in current after 450 s , which means that that there is some irregularity in the process of oxidation and reduction or the pores formation process is not uniform. Reference to figure 1 also shows irregular behavior of current at anodization temperature 30°C. The reason is that during anodization heat generates due to movement of ions towards the anode. Moreover, between 400 and 600 s, dissolution or reduction process dominates over oxidation process, and the number of ions involved in the movement towards the anode progressively increases. Later, oxidation process takes over reduction process, as indicated by progressive decrease in current. One can note that for a given anodization time, the amount of current increases, in general, with anodization temperature.
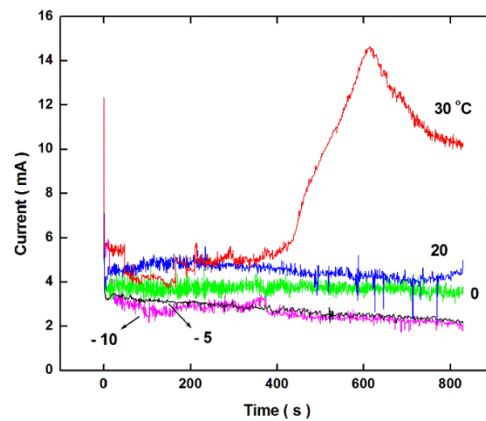
Fig. 1. Current – time plots of aluminium specimens anodized at –10, -5, 0, 20, and 30˚C.

3.2. Current density versus anodization temperature

Current density of anodization is defined as ratio of the total current involved in the anodization process and the area of specimen being anodized. The points in Fig. 2(a) and Fig. 2(b) denote the values of current density J and total charge transferred Q, respectively, as a function of anodization temperature. The lines drawn through the data points by least-squares fitting method represent an exponential growth in each case. It shows that mobility of electrolyte ions increases rapidly with anodization temperature between 0 to 30 ˚C.
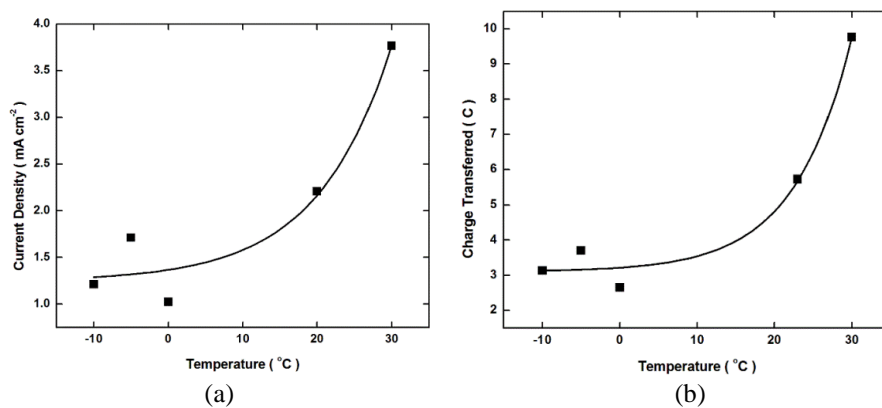

(a)   (b)

Fig. 2. Dependence of anodization current density (a) and charge transferred
(b) on the temperature of 0.3 M oxalic acid electrolyte

3.3. Film thickness

The film thickness of anodized specimens was calculated from Faraday's Law [18, 19]:

$$d = \frac{QM}{xy\,\rho\,FA} \tag{1}$$

Here d is the thickness of anodized film, $Q = \int_0^t I\,dt$ is the amount of charge passed, M (= 101.96 g mol^{-1}) is the molecular mass of Al$_2$O$_3$, x is the number of Al^{+3} ions in Al$_2$O$_3$ molecule, y is the number of O^{-2} ions in Al$_2$O$_3$ molecule, ρ (= 3.95 g cm^{-3}) is the density of Al$_2$O$_3$, F (= 96485 C mol^{-1}) is Faraday's constant, and A (= 2.16 cm^2) is the anodized area of the specimen. The values of film thickness (µm) of anodized specimens calculated by equation (1) have been denoted by points in Fig. 3(a) and Fig. 3(b) as a function of anodization temperature and total charge transferred, respectively. Least-squares fitting method was used to pass lines through the data points in each case. It is evident that film thickness increases exponentially with anodization temperature and linearly with charge transferred. Moreover, growth rate (nm min^{-1}) of thin films was calculated

from Faraday's Law, and was plotted as a function of current density J (mA cm^{-2}) in Fig. 3(c). A linear fit to the data points by least-squares fitting method shows that the growth rate of anodized films is directly proportional to the current density.
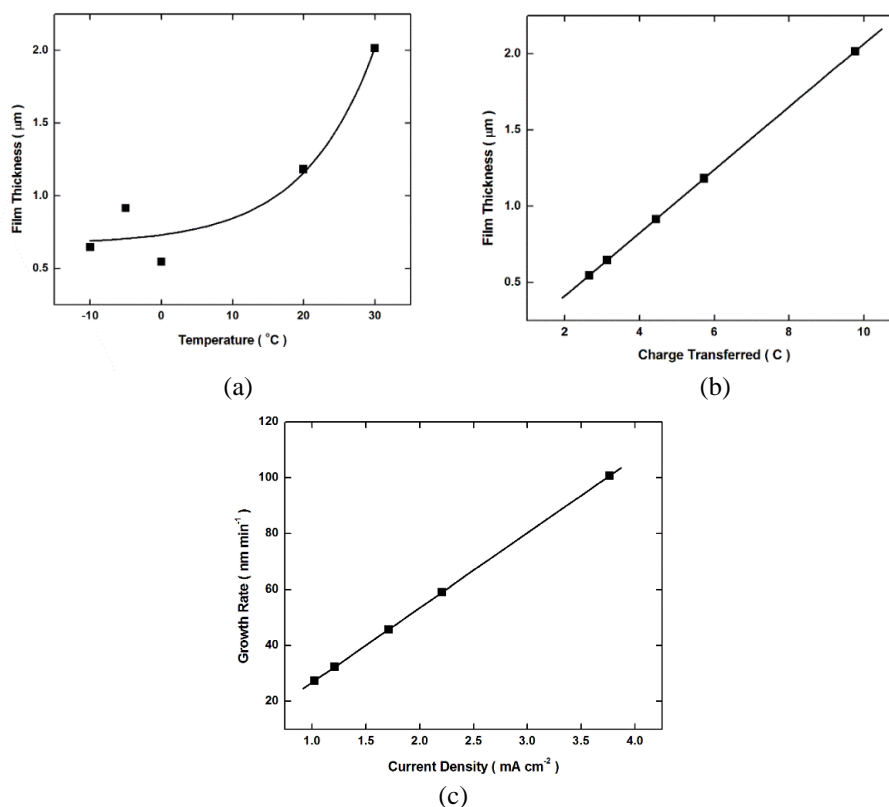

(a)

(b)

(c)

Fig. 3. Film thickness as a function of (a) anodizing temperature and (b) charge transferred.
(c) Growth rate of anodized film as a function of current density.

3.4. Rate process of anodization

To determine the activation energy E of rate process of anodization, the data pertaining to current density J, charge transferred Q, and film thickness d have been plotted as a function of inverse of anodization temperature T^{-1} in log-linear coordinates in Fig. 4. The straight lines fitted to data points in each case by least-squares fitting method are given by the expressions:

$$\ln J = 7.99 - 2071\, T^{-1} \tag{2}$$

$$\ln Q = 9.43 - 2218\, T^{-1} \tag{3}$$

$$\ln d = 7.36 - 2070\, T^{-1} \tag{4}$$

with linear correlation coefficient r = - 0.863, - 0.907, and - 0.863, respectively. The activation energy E of the rate process is found to be 0.182 eV with a standard deviation of 0.007.

It is pertinent to mention that Kashi and Ramazani [20] examined the effect of anodization temperature ($0 - 25^{\circ}$C) on the self-organized pore formation in anodic alumina. They used 5N pure aluminium as substrate in 0.3 M oxalic acid and anodization voltage was 40 V. It was found that the variation of current density with anodization temperature followed a typical exponential relation $J = J_{o} \exp(-E/kT)$ with $E = 0.44 \pm 0.01$ eV. The value of E measured by Kashi and Ramazani [20] is about two times higher than that measured in the present work. The difference may be attributed to the fact that anodization voltage used in the present work (50 V) is higher than the one (40 V) used by Kashi and Ramazani [20] in their experiment; higher anodization

voltage facilitates the anodization process and therefore reduces the activation energy E of the rate process of anodization.
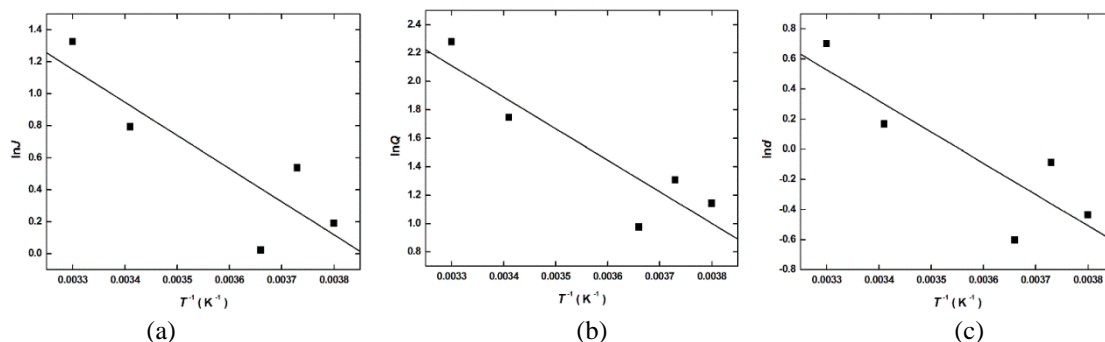

(a) (b) (c)

Fig. 4. Arrhenius plots of (a) current density J, (b) charge transferred Q,
and (c) film thickness d of anodized aluminium

3.5. SEM analysis

Surface morphology of aluminium specimens anodized at (a) −10, (b) − 5, (c) 0, (d) 20, and (e) 30 ℃ was studied by scanning electron microscope (Model: JSM-6480 LV, JEOL). SEM top-view image micrographs are given in   Fig. 5. Various structural parameters, namely pore diameter (D_P), interpore distance (D_i), pore density (n), pore circularity, and porosity (P) were measured from these micrographs with the help of Image J software.
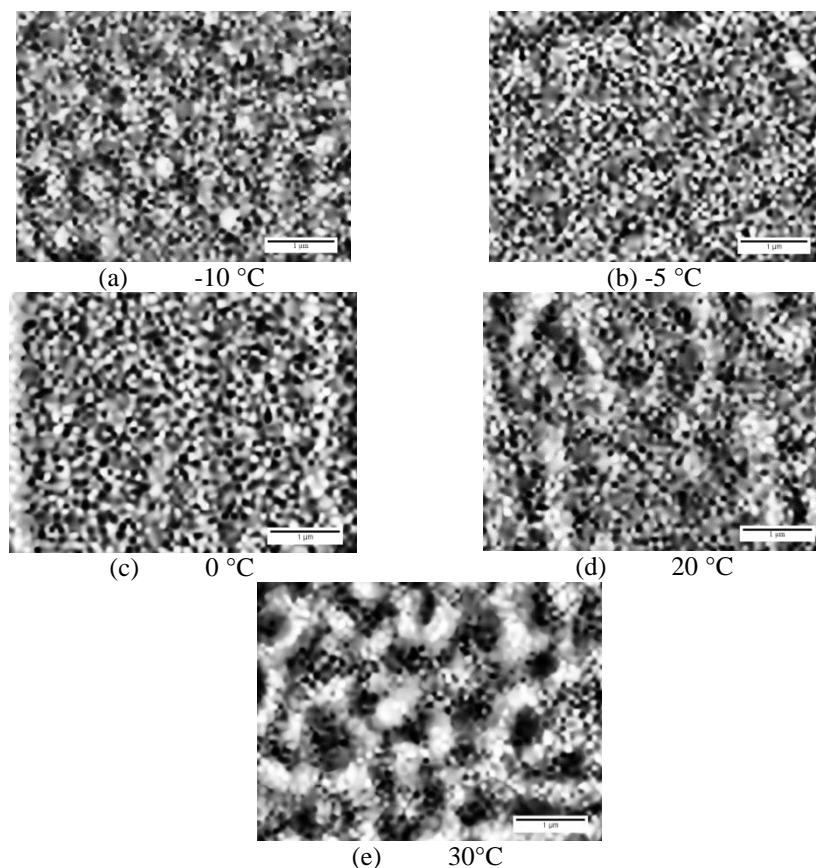

(a)   -10 °C

(b) -5 °C

(c)   0 °C

(d)   20 °C

(e)   30°C

Fig. 5. SEM top-view micrographs of porous alumina layer formed at various
anodization temperatures: (a) -10 °C, (b) ⬜5 °C, (c) 0 °C, (d) 20 °C, and (e) 30°C.

Referring to Fig. 6(a) and Fig. 6(b), pore diameter (D_P) increases linearly from 58 to 104 nm and interpore distance (D_i) increases from 137 to 165 nm with the increase in anodization temperature in the range – 10 ºC to + 30 ºC. Besides pore size, pore circularity is also an important factor for porous anodic aluminium oxide film. It is defined as [10]:

$$Circularity = 4\pi \frac{A}{S^2} \tag{5}$$

where A and S are area and perimeter of each pore. If circularity is 1, the pore shape is a perfect circle. The pore circularity in the present work lies in the range (0.763 – 0.859) and is maximum (0.859) at – 10ºC, as is evident from Fig. 6(c). One can also readily find pore density by means of the mathematical expression [21]:

$$n = \frac{2\times10^6}{\sqrt{3}\times D_i^2} \tag{6}$$

It is evident from Fig. 6(d) that pore density decreases linearly from 61.2 to 42.4 μm^{-2} with the increase in anodization temperature of electrolyte. It points to progressive merging of pores as anodization temperature is increased from – 10 to + 30 ºC. Using the values of pore diameter (D_P) and interpore distance (D_i), one can determine the porosity (P) of the aluminium oxide film from the formula [21]:

$$P = 0.907 \left(\frac{D_p}{D_i}\right)^2 \tag{7}$$

Reference to Fig. 6(e) shows that porosity (P) of the aluminium oxide film increases from 15.5 to 36.2% as anodization temperature is increased from – 10 to + 30 ºC. Finally, a comparison of Figs. 6(a), (b) and (d) shows that an increase in pore diameter and interpore distance is accompanied by a decrease in pore density. It may be pointed out that Zhang et al [22] has explicitly shown that circularity, regularity, and sharpness of the pores developed during first-step anodization of aluminium substrate improve on second-step anodization under the same conditions.
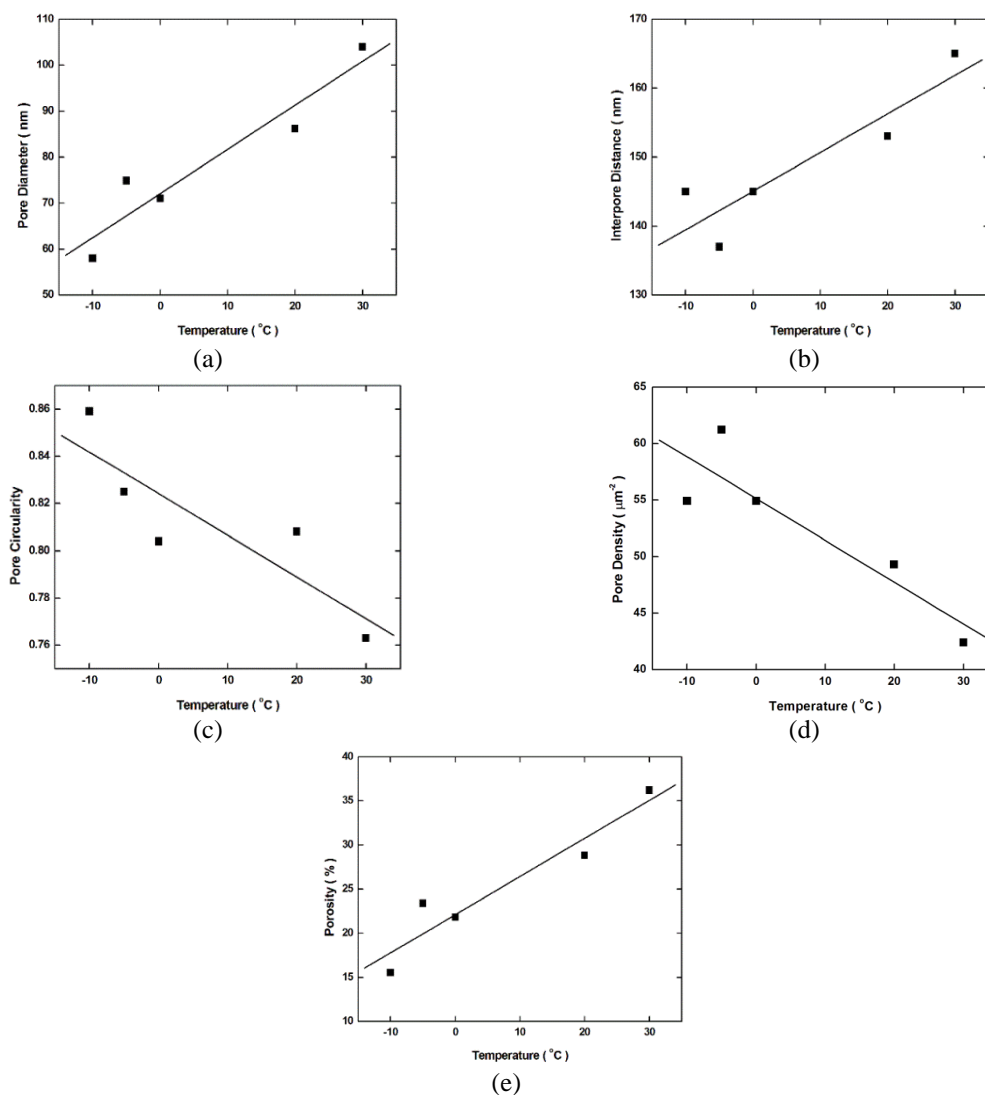
Fig. 6. Pore diameter (a), interpore distance (b), pore circularity (c), pore density (d), and porosity (e) as a function of anodization temperature.

3.6. Structural features of anodized aluminium substrate

XRD patterns of un-anodized and anodized aluminium specimens are shown in Fig. 7(a). All the noticeable peaks, on comparison with standard reference pattern (JCPDS: 01-089-4037), were indexed as (111), (200), (220), and (311). One can note that (111) and (200) peaks disappear on anodization.

3.6.1. Harris analysis

To determine the preferred orientation of un-anodized aluminium specimen, Harris analysis was performed using the following formula of texture coefficient [23, 24]:

$$P(h\,k\,l) = \frac{I(h\,k\,l)}{I_o(h\,k\,l)}\left[\frac{1}{n}\sum_{i=1}^{n}\frac{I(hkl)}{I_o(hkl)}\right]^{-1} \tag{8}$$

where I is the observed relative intensity with respect to the most intense diffracting plane and I_o is the standard relative intensity for $(h\,k\,l)$ planes obtained from JCPDS Card No. 01-089-4037 and n is the number of peaks in the diffraction pattern. For preferentially oriented plane, the $P\,(h\,k\,l)$ value should be greater than 1 [23, 24]. The texture coefficient of all four diffracting planes of un-anodized aluminium specimen obtained in this manner has been plotted as a function of 2θ in Fig.

7(b). One can readily see that the value of texture coefficient pertaining to (220) and (311) planes is greater than 1, while it is less than 1 for (111) and (200) planes.

Moreover, the points in Fig. 7(c) represents the peak intensity of preferentially oriented (311) plane of five anodized aluminium specimens as a function of anodization temperature. The horizontal line at 2047 cps level represents the peak intensity of (311) plane of un-anodized aluminium specimen. Suffice to say that the peak intensity of (311) plane of un-anodized Al specimen is decreased on anodization by 18 – 63%. According to simulation studies of Makinson et al [25], the peak intensity of x-rays diffraction peak of a crystallographic plane depends on the concentration of point defects in it. As the concentration of point defects (e. g. vacancies) increases, the peak intensity decreases. This points to the amorphous nature of the anodized film formed on the aluminium specimens.
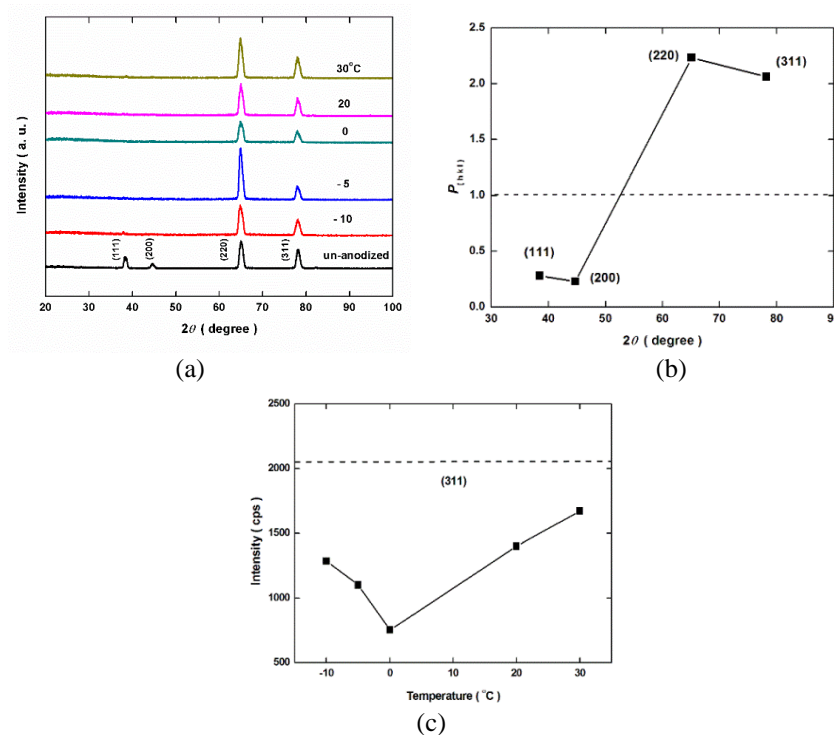

(a)

(b)

(c)

Fig. 7. (a) Combined XRD patterns of un-anodized and anodized aluminium specimens, (b) texture coefficient of various crystallographic planes of un-anodized aluminium specimen, and (c) peak intensity of preferred orientation plane (311) as a function of anodization temperature.

3.6.2. Williamson-Hall analysis

X-ray diffraction peaks broadening is caused by crystallite size (i.e. average size of coherently diffracting domains) and lattice strain, which can be analyzed by Williamson and Hall method [26, 27]. The mathematical expression for the full width at half maximum (FWHM) of a diffraction peak can be written as: $\beta = \beta_D + \beta_\varepsilon$, where β_D and β_ε are contributions to FWHM by crystallite size D and lattice strain ε, respectively. The peak broadening due to crystallite size D is given by Scherrer formula $\beta_D = \dfrac{k\lambda}{D \, Cos \, \theta}$, where λ is x – ray wavelength (= 0.15406 nm for CuK_α radiation) and $k \approx 0.9$ is shape factor. Contribution towards peak broadening by lattice strain ε is given by Wilson formula $\beta_\varepsilon = 4\varepsilon \, Sin \, \theta$. The FWHM of a diffraction peak is then given by the expression:

$$\beta = \frac{k\lambda}{D \, Cos \, \theta} + 4\varepsilon \tan \theta$$

or

$$\beta \cos \theta = \frac{k\lambda}{D} + 4\varepsilon \sin \theta \tag{9}$$

This is known as Williamson – Hall equation. One can also re-write equation (9) in an alternate form as:

$$\beta\cos\theta = A + B(4\sin\theta) \tag{10}$$

where $A = k\lambda/D$ and $B = \varepsilon$ are dimensionless constants.

Figs. 8(a) – (f) portray Williamson-Hall plots of un-anodized and anodized aluminium specimens for various anodization temperatures in the range −10 ºC to +30 ºC. The straight lines passed through the data points by least-squares fitting method are in accord with equation (10). The values of intercept A ($= k\lambda/D$) on y-axis and slope B ($= \varepsilon$) determined in this manner in each case are given in Table 1.
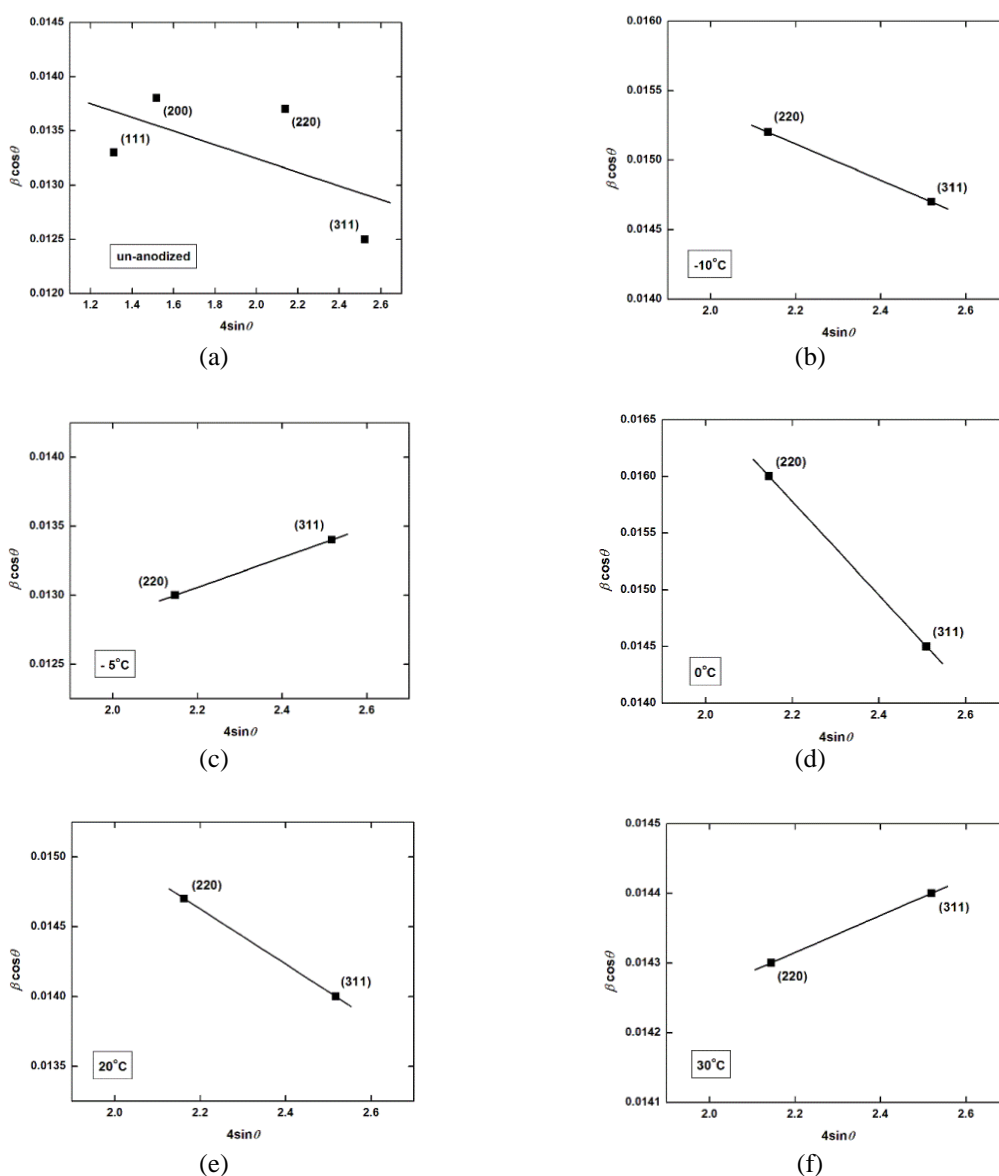

Fig. 8. Williamson – Hall plots of un-anodized and anodized aluminium specimens for various anodization temperatures in the range -10ºC to 30ºC.

Table 1. Structural data obtained by Williamson – Hall analysis

T (ºC)	A	B (= ε)	D (nm)
un-anodized	0.01451	− 0.00063	9.56
− 10	0.01797	− 0.00130	7.72
− 5	0.01068	0.00108	12.99
0	0.02484	− 0.00412	5.58
20	0.01896	− 0.00197	7.31
30	0.01373	0.00027	10.10

The values of crystallite size D and lattice strain ε (Table 1) of un-anodized and anodized aluminium specimens   have been depicted by points as a function of anodization temperature in Fig. 9(a). One can readily see that both D and ε vary with anodization temperature in an identical manner. The nature of lattice strain ε is compressive (–) for anodization temperatures – 10, 0, and 20 ºC and tensile (+) for – 5 and 30 ºC. The interdependence of D and ε has been illustrated in Fig. 9(b). The data pertaining to un-anodized aluminium specimen have also been included. Sigmoidal fit to the data points in Fig. 9(b) shows that lattice strain increases with the increase in crystallite size.
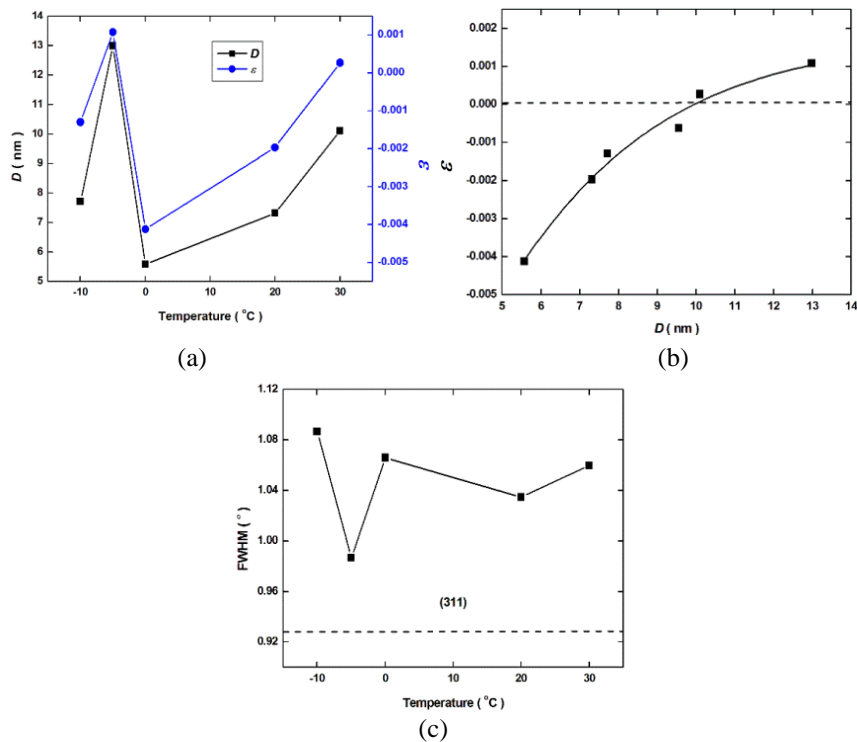

(a)

(b)

(c)

Fig. 9. (a) Crystallite size and lattice strain as a function of anodization temperature, (b) relationship between lattice strain and crystallite size, (c) FWHM of (311) diffraction peak as a function of anodization temperature.

Finally, points in Fig. 9(c) denote the values of FWHM of diffraction peaks of preferentially oriented (311) plane of five anodized aluminium specimens as a function of anodization temperature. The horizontal line at 0.92^o level represents the FWHM of (311) plane of un-anodized Al specimen. Suffice to say that the FWHM of (311) plane of un-anodized aluminium specimen is increased on anodization by 6.6 to 17.3%. According to Ungar [28], x-ray diffraction peaks are broadened if lattice defects, e.g. point defects like vacancies, are considerably increased. This trend is consistent with the observations portrayed in Fig. 7(c) that the peak intensity of preferentially oriented (311) plane of five anodized aluminium specimens decreases with the increase in anodization temperature due to increase in the concentration of point defects in it. Thus a decrease in the peak intensity of x-rays diffraction peak of a crystallographic plane due to increase in vacancy concentration is accompanied by an increase in FWHM or peak broadening of the diffraction peak.

4. Conclusions

First-step anodization of commercial aluminium in 0.3 M oxalic acid at 50 V for 15 min was carried out at –10, –5, 0, 20, and 30 ºC. It is observed that current density (1.02 mA cm^{-2} – 3.77 mA cm^{-2}), charge transferred (2.65 C – 9.76 C), and thickness of porous alumina film (0.547 μm – 2.015 μm) increase exponentially with anodization temperature. The activation energy of the rate process of anodization determined from the Arrhenius plots of current density, charge transferred, and film thickness is found to be 0.182 eV with a standard deviation of 0.007 eV. Structural features of porous alumina examined by SEM show that pore diameter (58 nm to 104 nm), interpore distance (137 nm – 165 nm), and porosity (15.5% to 36.2%.) increase whereas pore circularity (0.763 – 0.859) and pore density (61.2 μm^{-2} – 42.4 μm^{-2}) decrease linearly with the increase in anodization temperature. Similarly, XRD studies of anodized commercial aluminium substrate reveal that the intensity of diffraction peak pertaining to preferentially oriented crystallographic plane (311) is decreased whereas its FWHM is increased at all anodization temperatures. The observations are in qualitative agreement with those reported in the literature for high-purity aluminium.

References

[1] G.D Sulka, K.G Parkoła, Electrochim. Acta. **52,** 1880 (2007).
[2] Y. Zuo, Y. Zhao,X. Li,N. Li,X. Bai, S.S Qiu, Mater. Lett. **60,** 2937 (2006).
[3] M. P. Proenca, C.T Sousa, D.C Leitao, J. Ventura, J.B Sousa, J.P Araujo, J. Non-Cryst. Solids. **354,** 5238 (2008).
[4] A.O Araoyinbo,A. Rahmat, M.N Derman, K.R Ahmad, Adv. Mater. Lett. **3**, 273 (2012).
[5] U. Yogeswaran, S.M Chen, Sensors. **8**, 290 (2008).
[6] Z. Huang,W. Zhang, J. Yu, D. Gao, J. Med. Device. **1**, 79 (2007).
[7] A.M Abd-Elnaiem, A. Gaber, Int. J. Electrochem. Sci. **8**, 9741 (2013).
[8] S. Altuntas, F. Buyukserin, Appl. Surf. Sci. **318**, 290 (2014).
[9] M. Jayalakshmi, K. Balasubramanian, Int. J. Electrochem. Sci. **3**, 1196 (2008).
[10] C.K Chung, M.W Liao, H.C Chang, C.T Lee, Thin Solid Films. **520**, 1554 (2011).
[11] W.J Stępniowski, Z. Bojar, Surf. Coat. Technol. **206**, 265 (2011).
[12] C.K Chung, W.T Chang, M.W Liao, H.C Chang, C.T Lee, Electrochim. Acta. **56**, 6489 (2011).
[13] D.Y Hwang, Y.M Kim, D.H Shin, Mater. Trans. **50**, 671 (2009).
[14] S.H Su, C.S Li, F.Bin Zhang, Yokoyama M, Superlattices Microstruct. **44**, 514 (2008).
[15] A.W Juyana, M.N Derman, Adv. Mater. Res. **173**, 55 (2010).
[16] Y. Jia,H. Zhou,P. Luo, S. Luo, J. Chen, Y. Kuang, Surf. Coat. Technol. **201**, 513 (2006).
[17] G.D Sulka, W.J Stepniowski, Electrochim. Acta. **54**, 3683 (2009).
[18] J.W Diggle, T.C Downie, C.W Goulding, Chem.Rev. **69,** 365 (1969).
[19] Hariom, N. Verma, K.C Singh, Europ. J. Appl. Engg. Sci. Res **2,** 25 (2013).

[20] M. A.Kashi, A.Ramazani, J. Phys. D:Appl. Phys. **38,** 2396 (2005)

 [21] G. E. J. Poinern, N. Ali, D. Fawcett, materials **4**, 487 (2011).

[22] S. Zhang, Y.Wang, Y.Tan, J.Zhu, K.Liu, J.Zhu,Mat. Res. Exp. **3,** 074004 (2016).

[23] C. S. Barret, T.B Massalski. Structure of Matals. Oxford:Perrgamon. (1980).

[24] M.Z Butt,D. Ali, M. Aftab, M.U Tanveer, Surf. Topogr: Metrol.Prop **3**, 35002 (2015).

[25] J.D Makinson, J.S Lee,S.H Magner, R.J De Angelis, W.N Weins, A.S Hieronymus. Advances in X-ray Analysis. **42** ,407 (2000).

[26] G. K. Williamson,W.H Hall, Acta Metall. **1**, 22 (1953).

[27] M. Z. Butt, M.W Khaliq, A.M Majeed D. Ali, Mat. Res. Exp **3**, 096503 (2016)

[28] T. Ungar, Scr. Mater **51**, 777 (2004).